ELSEVIER

Journal of Molecular Catalysis A: Chemical 112 (1996) 413–421

JOURNAL OF MOLECULAR CATALYSIS A: CHEMICAL

Analysis by size exclusion chromatography (SEC) of catalytic materials: The fractal properties and the pore size distribution of pumice

Dario Duca *, Giulio Deganello

Istituto di Chimica e Tecnologia dei Prodotti Naturali del CNR and Dipartimento di Chimica Inorganica, Università di Palermo, Via Archirafi 26-28, 90123 Palermo, Italy

Received 20 November 1995; accepted 29 April 1996

Abstract

Size exclusion chromatography (SEC), a technique usually employed as preparative and/or analytical tool, gives more insights on the morphology of pumice, a natural amorphous alumino–silicate recently reproposed as support for metal catalysts. The SEC analysis of pumice is based on benzene and a set of 13 polystyrenes ($700 \leq$ uma $\leq 1{,}500{,}000$) as standard probes. A modelistic approach which can detect fractal properties of the materials is presented. SEC confirmed the main physical characteristics of pumice, determined by other techniques, and, in addition, showed that a bidistribution of pore size and fractal properties are present in pumice. Since SEC is performed in liquid phase, it could become an interesting tool for the characterization of the catalytic materials employed in liquid phase reactions.

Keywords: Size exclusion chromatography; Catalyst support characterization; Pumice; Metal supported catalyst; Surface

1. Introduction

The pumice of Lipari was recently reproposed as support for metal catalysts [1] on the basis of interesting results obtained with metal/pumice catalysts in the selective hydrogenation of dienes [2,3] and alkynes [4–6]. The chemical composition of pumice is close to that of natural zeolites, but opposite to zeolites, pumice is amorphous. Recently, the structure of pumice was studied by X-ray photoelectron spectroscopy (XPS) and ^{27}Al magic angle spinning nuclear magnetic resonance (^{27}Al MAS NMR) [7] and wide angle neutron scattering (WANS) [8]. Pumice grains < 45 μm have a low surface area [1] (< 5 m^2 g^{-1}) and a relatively high 'apparent' density [9] (2.35 g cm^{-3}). Gas adsorption methods (BET-surface area and BJH method) and small angle X-ray scattering (SAXS) analyses [1] indicate that pumice is a non-porous material with smooth surface, whereas SANS and WANS analyses [8] suggest that pumice presents a large number of pores with dimensions that are mainly ranging between 30 and 500 Å. The presence of Na^+ and K^+ in the framework of pumice seems to be relevant in promoting some unusual properties in metal/pumice catalysts. Thus, Pd/pumice showed good activity in the hydrogenation of

* Corresponding author. Fax: +39-91-6166281; e-mail: dduca@ipacuc.cuc.unipa.it.

PII S1381-1169(96)00181-1

highly unsaturated hydrocarbons [2–6] up to large metal dispersions whereas Pd supported on more traditional oxides (silica and alumina) showed a drastic decrease in activity at metal dispersions higher than 20% [10,11]. Interestingly, a shift of Pd 3d binding energies towards negative values was determined in Pd/pumice catalysts [12,13] suggesting a transfer of electronic density on the supported metal. Recently these shifts in addition to the Auger energy shifts were employed to estimate the electron density on the Pd particles of the Pd/pumice catalysts and a nice correlation was found [14] between electron density on the pumice-supported Pd particles and catalytic activity. Moreover, for the first time, in the case of pumice supported Pd catalysts, stacking-faults [15–17] were detected. At present we do not know whether stacking-faults features are related to the peculiar influence of the support or to the method of preparation of the catalysts. In the present study we present deeper insights on the morphological properties of pumice by SEC [18,19], and we hope to show the potentiality of this technique in the analysis of materials of interest in catalysis.

2. Size exclusion chromatography (SEC)

The use of a chromatographic method for the determination of morphological data of porous solids, already considered since 1960, was developed by Halász and Martin [20] in 1970. Since the theoretical basis of the technique and the different approaches to the interpretation of experimental data are well documented in literature [19,21–23], here we remind only some necessary concepts.

2.1. General aspects

The determination of porosity by SEC requires high performance liquid chromatography (HPLC) equipment. The solvents used (i.e., the mobile phase in chromatography), usually have a polarity ranging between that of water and that of tetrahydrophuran (THF). The sample of the material is packed with dry or slurry methods in the stainless steel tubes used in HPLC.

The porous structure of the sample sieves the standard probe molecules solubilized in the mobile phase. No interactions are assumed to take place between the solutes and the material [18] and the retention time of the different molecules is therefore related to their rates of migration through the pores of the material. Although there are some disagreements about the mechanism of separation [24], its correlation on the specific distribution of molecule solutes between mobile and stationary phase is widely accepted. The sizes of the probe molecules and the sizes of the pores are responsible for the above distribution. Therefore, the smallest probe (e.g. benzene) pass through the largest number of pores [18], while molecules of larger size pass through a smaller portion of the above pores. The retention time is greater [18] for smaller molecules and therefore, the elution of the probe molecules [24] starts with the largest ones.

Since SEC analysis is based on the interaction between liquid and solid phases, it is likely that SEC can be preferred to other techniques in the study of catalytic materials employed in liquid phase reaction.

Besides benzene, the usual standard probes in the analysis of rigid materials are styrene polymers of different molecular weight [20]. These polymers are considered as non-deformable spherical particles. An approximate empirical relation between the molecular weight (M_w) of these probe molecules and their effective 'hard sphere' diameters (φ) (i.e., the apparent diameter of the probe molecule in the solvent) was proposed [25]. Thus, for the generic i-th probe molecule:

$$\varphi_i = a(M_w)_i^{\alpha}. \quad (1)$$

Although the values of a and α, the empirical parameters, are reported by different authors [20,25,26], it is preferable to determine them by

standardizing the own system [25] using materials of known morphology.

Eq. (1) is fundamental in SEC analysis together with the formal definition of the elution volume V_{ei} [25] for the generic i-th probe molecule:

$$V_{ei} = V_j + K_i V_\pi \tag{2}$$

where V_j represents the interparticle volume, V_π the intraparticle volume and K_i the exclusion coefficient [25] $(0 \leq K_i \leq 1)$ of the i-th molecule. K_i gives the fraction of the intraparticle volume explored by the probe molecule. The elution volume for a generic molecule i, having an effective diameter φ_i, is a cumulative volume determined by the pores of the sample with an accessible diameter [27] larger or equal to φ_i. Therefore, Eq. (2) is suitable only if the size of the largest probe molecules inhibits its exploration of the intraparticle volume, but it allows the exploration of the interparticle volume; in other words, the exclusion coefficient is 0 for the largest probe.

2.2. Modelistic approach

Although a neutron diffraction study could not detect volume fractality for pumice, the existence of fractal characteristics in this material was not ruled out [8]. To verify this possibility a modelistic approach [18,28], amenable to detect, if present, fractal characteristics [29,30] of the materials was employed in this SEC study of pumice.

In place of the availability coefficient [18] usually employed in fractal modeling, we used the exclusion coefficient [25] which is related by a constant to the first one.

The relation between the exclusion coefficient K_i and the molecular weights $(M_w)_i$ of the probes is:

$$K_i = \mu (M_w)_i^b. \tag{3}$$

It is important to underline that K_i is also the pore-volume [9], cumulative volume per gram of the material, detected by molecules with molecular weight $(M_w)_i$ normalized to the total pore-volume of the porous solid. μ is a shape factor related to the morphological characteristics of the material and b is a parameter related to the fractal dimension [29,30] characterizing self-similar systems.

If M_w is a non-discrete continuous variable, from Eq. (3) one can obtain:

$$\mathrm{d}K/\mathrm{d}(M_w) = bK/(M_w). \tag{4}$$

In real systems the value determined by different probes and connected to a measurement of a morphological property of a material has a lower (L) and an upper (U) limit. Therefore, for non-ideal systems [18,28]:

$$\lim_{K \to L} (\mathrm{d}K/\mathrm{d}(M_w)) \to 0 \tag{5a}$$

$$\lim_{K \to U} (\mathrm{d}K/\mathrm{d}(M_w)) \to 0. \tag{5b}$$

In the present case, these limits are determined by probes that cannot detect the studied property above a limit value of M_w, and probes that detect it in all the details below another and opposite limit value of M_w. Therefore, according to Sernetz et al. [18,28] we used:

$$\mathrm{d}K/\mathrm{d}(M_w) = [b(U-K)(K-L)] / [(U-L)(M_w)] \tag{6}$$

in place of Eq. (4), since it asymptotically tends to 0 when $K \to U$ or $K \to L$ and, therefore, it is more appropriate in representing a real situation.

Integration of Eq. (6) gives the analytical expression of the exclusion coefficient employed in our modelistic approach:

$$K = U\{1 - [1 - L/U] / [1 + \exp[b(\ln(M_w) - Q)]]\} \tag{7}$$

where $K[\ln(M_w)]$ is a sigmoid function with a slope determined by b and with the inflection point at $\ln(M_w) = Q$.

The volume fractal properties of a material using SEC technique can be determined by the analysis of the physical properties related to the solid–liquid interface of the material [18]. The

function $K[\ln(M_w)]$ which does not contain any information on the solid–liquid interface of the material [18], is not useful to this purpose. However, by scaling the cumulative non-available pore-volume:

$$(U-K)/(U-L) = 1/\left[1+\exp\left[(3-D)(\ln(M_w)-Q)\right]\right] \quad (8a)$$

obtained from Eq. (7) and including the solid–liquid interface [18], it is possible to determine D (the fractal dimension of the material). If, however, as in the case of pumice (see below), different pore-volume distributions overlap into the material, in order to avoid any influence of the overlapping, the fractal dimensions are determined [18] by scaling the following equation:

$$(U-K)/(K-L) = \left\{\left[(M_w)-(M_w)_m\right] / \left[(M_w)_M-(M_w)\right]\right\}^{3-D} \quad (8b)$$

where $(M_w)_m$ and $(M_w)_M$ are the lower and the upper cut-off inside limits of the considered fractality range, respectively.

The validity of Eq. (8b), employed in this work is supported by experimental studies and by computer simulations [18]. For the sake of simplicity, from now on Eq. (8b) will be represented as $\Gamma = \Xi^{3-D}$.

Since for generic materials the surface detected by the probe molecule with effective 'hard sphere' diameter φ is $S(\varphi) = |V_\pi(\mathrm{d}K/\mathrm{d}\varphi)|$, the total surface of the material in our study was obtained by considering the $S(\varphi)$ value originated by the smallest probe molecule (i.e., the molecule which detects all the total pore-volume present in the material). Furthermore, $|\mathrm{d}V| = |V_\pi \mathrm{d}K(\varphi)|$ is the differential cumulative volume, that is, the difference between the volume detected by a probe with a diameter φ and that detected by a probe with a diameter $\varphi + \mathrm{d}\varphi$. Then, setting $\mathrm{d}\varphi$ at a value sufficiently small, the pore size distribution [9] related to the total amount of the material can be graphically represented by $|\mathrm{d}V|/\mathrm{d}\varphi$ versus $\varphi + \mathrm{d}\varphi/2$.

In conclusion, in this work, the theoretical trend of K and the related parameters were determined by a fit of a mathematical model to the experimental K versus $\ln(M_w)$, and, the fractal properties as well as the specific surface area and the pore size distribution of the material were determined using the above reported equations of $S(\varphi)$ and $|\mathrm{d}V|/\mathrm{d}\varphi$.

3. Experimental

The HPLC apparatus (GILSON) was equipped with a Piston pump type 302, a HM Holochrome UV/Vis detector, set on 254 μm, a Manometric module type 802, and an Automatic Sampler type 232–401.

The elution time of each standard probe was measured at the maximum of the peak and the elution volume was obtained by multiplying time per elution flow.

The reagents used have HPLC purity grade. Tetrahydrofuran (THF) (Koch Light) was used as eluent phase. 0.2% solutions in THF of benzene (Ph) (Aldrich) and a set of thirteen polystyrene standards (Aldrich) with molecular weight within a range of 700 and 1,500,000 uma, were used as probes.

The pumice (grain dimension < 45 μm) was purified before analysis according to a published procedure [17]. After this treatment, the pumice (3.8964 g) was packed in a HPLC stainless steel tube (250 mm $\times$ 4.6 mm, effective column volume 4.2415 ml) by a slurry method [31]. The column was thermostated at 298 K.

Pumice was washed with THF until a stable pressure was reached (~ 6 h) in the column (15 ± 1 bar) and the flow of the eluent phase during the experiments was set at a very low value (0.25 $\mathrm{cm^3\ min^{-1}}$). In order to have sound statistics, at least 10 analyses were performed for every i-th probe molecule. Moreover, every analysis was composed of three different

Table 1
Characteristics of the probe molecules

Probe	Molecular weight M_w (uma)	Rigid sphere diameter φ_{Ni} [a] (nm)
Ph	78	0.53
S_1	687	1.92
S_2	2,700	4.29
S_3	4,075	5.47
S_4	9,100	8.77
S_5	24,150	15.56
S_6	32,660	18.58
S_7	45,730	22.65
S_8	95,800	34.99
S_9	184,200	51.39
S_{10}	401,304	81.23
S_{11}	573,000	100.16
S_{12}	850,000	126.30
S_{13}	1,447,000	172.68

[a] Label Ni underlines that these rigid sphere diameters are obtained using the a and α values suggested by Nikolov [25].

molecule injections (5 μl of solution) in times exactly prefixed. The first injection was always that of the largest probe that evaluated V_j, the last always that of the smallest one (Ph), that, in first approximation, evaluated $V_j + V_\pi$ and the middle the one of the considered probe, that evaluated V_{ei}. This procedure allowed to have for every analysis a self-determined value of K (see Eq. (1)). The averaged standard deviation on the experimental values of K was 0.008. The values of $a = 0.0412$ and $\alpha = 0.588$ employed in Eq. (1) in order to have the hard sphere diameters of the molecules were those suggested by Nikolov [25]. In fact, the SEC analysis performed on two standard products (silica-gel Davisil standard grade (Aldrich), grain dimension < 20 μm, surface area 480 m^2 g^{-1}, pore-volume 0.75 cm^3 g^{-1})) and (alumina standard grade (Aldrich), grain dimension $<$ 130 μm, surface area 150 m^2 g^{-1}), using the above Nikolov parameters and the reported experimental conditions gave results with less than 5% deviation from those reported in literature. The symbols of the probe molecules employed in this work, their molecular weights M_w and the corresponding hard sphere diameters φ_{Ni} are reported in Table 1.

All the computing procedures of this work were performed using FORTRAN programs in house developed.

4. Results and discussion

Usually the smallest probe used in the morphological characterization by SEC is benzene. Therefore, if V_π (the intraparticle volume) is determined by the elution volume of benzene, pores with a diameter smaller than 0.5 nm (see Table 1) are arbitrarily excluded. To avoid this, an extrapolation, using POLINT on four points [32], of the elution volume value of a hypothetical probe having a hard sphere diameter tending to zero was performed. The total pumice pore-volume (total volume of the pores in the pumice) obtained is about 5% larger than that obtained using benzene as the smallest probe. The above procedure was applied also to hypothetical probe molecules with hard sphere diameters smaller than 0.3 nm. Since, however, the value of the total pumice pore-volume did not increase further, pore diameters smaller than 0.3 nm were ruled out in pumice.

In Fig. 1 the experimental values of K determined considering Eq. (2) are reported together

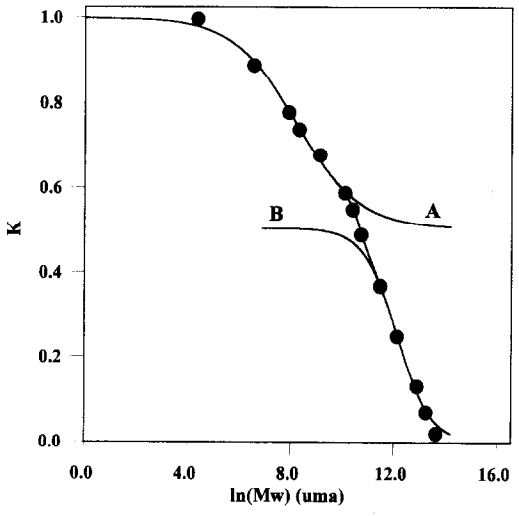

Fig. 1. K versus $\ln(M_w)$. Plot of the exclusion coefficients versus the logarithm of the probe molecular weights. ● experimental points and fitting curve. Curves A and B are the contributions K_1 and K_2, respectively, to K in Eq. (9).

with the fitting curves (see below). The value of V_π is obtained by the above mentioned extrapolation, while V_j is determined by the elution volume of probe molecule S_{13}. The points of Fig. 1 fit on a curve resulting by a combination of two sigmoids; in SEC analysis, two different distributions of pore-volume [18,33] are assumed when the above conditions occurs. These distributions can be related to inter- and intra-particle [18] pore-volume or to a bidistribution of intra-particle [33] pore-volumes. Since the sizes of the pumice grains are about two order of magnitude greater than the sizes of the largest pores detected, and the inter-particle pores are like to have sizes comparable to those of the grains, inter-particle pore-volume can be excluded. In order to study this intra-particle bidistribution of pore-volumes, Eq. (7) is modified as follows:

$$K = f_1 K_1 + f_2 K_2 \tag{9}$$

where K_1 and K_2 are both equal to K of Eq. (7), although working in two different ranges of pore-volume. Their upper and lower limits are different as well as their fractal dimensions and inflection points. Moreover, $0 \le f_1 \le 1$ and $f_2 = 1 - f_1$ are Fermi functions driving the transition from one to the other range of pore-volume and:

$$f_1 = 1/\{1 + \exp \beta[\ln(M_w) - \varphi_I]\} \tag{10}$$

where φ_I is the intermediate value in the range of transition between the two pore-volume distributions and β is a parameter that determines the rapidity of the above transition. In a first attempt, 6 parameters were employed to fit Eq. (9) to the experimental K versus $\ln(M_w)$. Then, besides β and φ_I of the Fermi functions, the upper U and lower L limits in the two pore-volume ranges were considered. However, the upper U_1 limit of the first pore-volume range had a value closely to 1 while the value of the lower L_2 limit of the second pore-volume range is practically 0. Moreover, both, the lower L_1 and upper U_2 limits, had values closely to $K(\varphi_I)$. Assuming $U_1 = 1$, $L_2 = 0$ and $L_1 = U_2 = K(\varphi_I)$, the model fitted the experimental data only with the two parameters of the Fermi functions. The calculation of the various parameters was performed according to the following procedure:

(a) Application of a SIMPLEX procedure [32], in order to select the two fitting parameters β and φ_I.

(b) Employing the experimental values of K and the interpolated value of $K(\varphi_I)$, POLINT procedure [32], use of the logit transformation [34] of Eq. (7):

$$\ln[(K - L)/(U - K)] = b[(\ln(M_w) - Q)] \tag{11}$$

in the two range of pore-volume distribution in order to determine the parameters b_1, b_2, Q_1 and Q_2.

(c) Use of Eq. (9) in order to calculate $K(M_w)$, the goodness of fitting was given by comparison of the experimental and calculated K values through a χ^2 function.

(d) Use of the SIMPLEX [32] in order to test if the imposed limits of convergence in the fitting are achieved or not and then if the fitting procedure (point *a*) was to be continued or not.

The parameters obtained by the above operations are reported in Table 2, and the fitting curve in Fig. 1. Curves A and B represent the contribution of K_1 and K_2, respectively, to the fitting curve.

Since the value of β parameter is great, the transition between the two range of pore-volume is fast, supporting the $L_1 = U_2 = K(\varphi_I)$ imposition. b parameter gives the dispersion of the K

Table 2
Calculated parameters [a]

χ^2	$1.45940(8) \times 10^{-4}$
β	5.184(9)
φ_I	$1.0647(6) \times 10^{1}$
$L_1 = U_2$	$5.036(2) \times 10^{-1}$
b_1	$-8.038(1) \times 10^{-1}$
Q_1	8.1949(8)
b_2	−1.5370(8)
Q_2	$1.21299(8) \times 10^{1}$

[a] For the meaning of the symbols see text.

distribution [18], i.e. the normalized pore-volume distribution, and, according to the values of Table 2, the second pore-volume range has a dispersion almost double of that of the first pore-volume range. The maximum of the normalized pore-volume distributions, obtained from the values of Q, i.e., from the position of the inflection points of K_1 and K_2, and, reported as hard sphere diameters φ, resulted 5.1 and 51.6 nm, respectively.

By introducing into the Eq. (8b), the calculated points of K_1 and K_2 and assuming as molecular weights of the probes the cuts-off 650–6,000 uma for the first pore-volume range ($0.90 \geq K_1 \geq 0.65$) and 133,850–795,000 uma for the second pore-volume range ($0.30 \geq K_2 \geq 0.05$), the fractal dimensions of the two ranges of pore-volume, were determined from the slope of the curves $\log(\Gamma)$ versus $\log(\Xi)$ (Fig. 2), as 2.02 ($R = 0.99998$) and 1.95 ($R = 0.99990$), respectively. The fractal properties and the bidistribution of pore-volume in pumice could not be detected by other techniques.

The pore size distribution related to the total amount of the material $|dV(\varphi)|/d\varphi$ versus $\varphi + d\varphi/2$ is shown in Fig. 3. The intraparticle

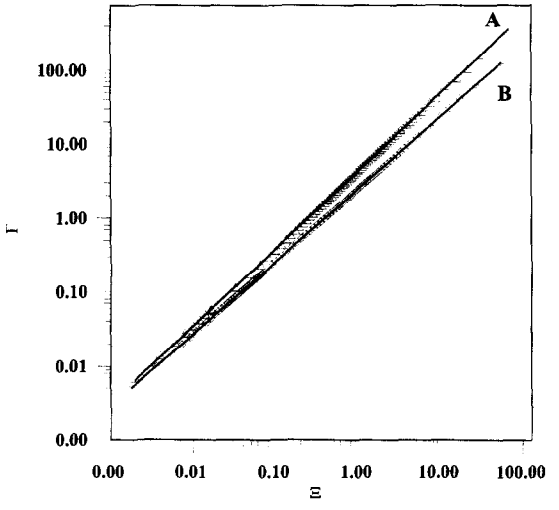

Fig. 2. Γ versus Ξ in logarithmic scale, log–log plot of the truncated distribution according to Eq. (8b). △ and ◇ are points obtained from the calculated points of K_2 and K_1, respectively, employing the probe molecular weights 133,850–795,000 and 650–6000 uma as cutoffs for the two pore-volume ranges. Straight lines A and B, respectively, fit △ and ◇ points.

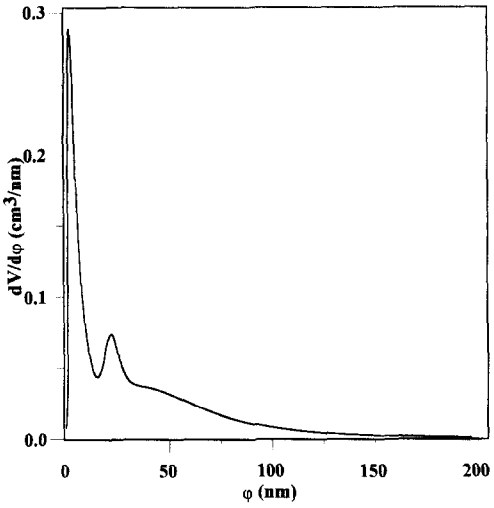

Fig. 3. Pore size distribution in pumice: $|dV|/d\varphi$ versus $\varphi + d\varphi/2$. $|dV|$ is the differential cumulative volume due to pores with diameters in the range of sizes φ and $\varphi + d\varphi$, $d\varphi = 0.02$ nm.

volume of pumice is mainly due to micro-pores (maximum at 1.2 nm); however, a small maximum (at 21.5 nm) in the region of meso-pores and intra-particle volume due to macro-pores is also present (Fig. 3). The large distribution of pore size, here found in the pumice, confirms previous results [8] obtained by a neutron scattering study.

The interparticle volume, V_j, of our system resulted 2.62 cm^3 while the intraparticle volume, V_π, resulted 0.24 cm^3.

Employing the equation $S(\varphi) = |V_\pi(dK/d\varphi)|$, the surface of pumice in the column was determined considering an hypothetical probe with a hard sphere diameter $\varphi = 0.3$ nm. This cumulative surface 7.6 m^2 normalized to the amount of pumice in the column gives 1.95 $m^2\ g^{-1}$ as specific surface area. The 'apparent' density d of pumice, known the volume of the column V_c and the weight of the material W_m, was obtained by $d = W_m/(V_c - V_j)$ as 2.40 $g\ cm^{-3}$, while the total porosity, ε [9], obtained by $\varepsilon = V_\pi/(V_c - V_j)$ resulted 0.15.

Besides the pore size distribution, the low value of total porosity and the specific surface area as well as the value of density of pumice are in accord with our previous results obtained

by other techniques [7,8]. The low total porosity of pumice determined in this study suggests that porous are mainly on the surface of the support. This hypothesis is well in agreement with the values of the fractal dimension found and, therefore, it is easy to speculate that the surface roughness could condition the growing on pumice of the first layers of metal crystallites thus originating the stacking-faults formed in pumice-supported Pd and Pt catalysts [15–17]. In addition kinetic studies on three phase (gas–liquid–solid) reactor systems employing pumice-supported metal catalysts [2–6] do not suffer dramatically by mass transfer limitation, probably owing to the absence of intraparticle diffusion phenomena.

5. Conclusions

Although the low surface area and the presence of pores in the pumice were already established [8], this study shows for the first time the surface bimodal distribution of these pores and the fractal properties of pumice. The high number of surface micropores on pumice can explain the presence of stacking-faults found by X-ray diffraction techniques [17–19] in pumice supported Pd and/or Pt catalysts. The low pore-volume of pumice, being localized on the surface does not cause dramatic mass transferring problems in catalytic reactions with metal/pumice catalysts; the surface pore-volume of pumice, however, can influence the modality of growing of the metal crystallites on the support.

The SEC technique is, therefore, a useful tool for the characterization of supports and could be an interesting alternative or at least an additional technique for studies of porous materials used in catalysis.

Acknowledgements

We thank CNR (Progetto Finalizzato "Chimica Fine II" and Progetto Strategico "Tecnologia Chimiche Innovative") and Ministero dell'Università e della Ricerca Scientifica e Tecnologica. (MURST 40%) for the financial support, and PUMEX S.p.A. for supplying pumice samples.

References

[1] G. Deganello, D. Duca, L.F. Liotta, A. Martorana and A.M. Venezia, Gazz. Chim. Ital. 124 (1994) 229.
[2] G. Deganello, D. Duca, A. Martorana, G. Fagherazzi and A. Benedetti, J. Catal. 150 (1994) 127.
[3] G. Deganello, D. Duca, L.F. Liotta, A.M. Venezia, A. Martorana, G. Fagherazzi and A. Benedetti, J. Catal. 151 (1995) 69.
[4] D. Duca, L.F. Liotta and G. Deganello, J. Catal. 154 (1995) 113.
[5] D. Duca, L.F. Liotta and G. Deganello, Catal. Today 24 (1995) 15.
[6] D. Duca, A. Parmaliana, F. Frusteri and G. Deganello, Appl. Catal., in press.
[7] A.M. Venezia, M.A. Floriano, G. Deganello and A. Rossi, Surf. Interface Anal. 18 (1992) 532.
[8] M.A. Floriano, A.M. Venezia, G. Deganello, E.C. Svensson and J.H. Root, J. Appl. Cryst. 27 (1994) 271.
[9] J. Rouquerol, D. Avnir, C.W. Fairbridge, D.H. Everett, J.H. Haynes, N. Pernicone, J.D.F. Ramsay, K.S.W. Sing and K.K. Unger, Pure Appl. Chem. 66(8) (1994) 1739.
[10] J.P. Boitiaux, J. Cosyns and S. Vasudevan, in: Preparation of Catalysts III, P. Poncelet, P. Grange and P.A. Jacobs (Eds.) (Elsevier, Amsterdam, 1983) p. 123.
[11] J.P. Boitiaux, J. Cosyns and S. Vasudevan, Appl. Catal. 6 (1983) 4.
[12] A.M. Venezia, D. Duca, M.A. Floriano, G. Deganello and A. Rossi, Surf. Interface Anal. 18 (1992) 619.
[13] A.M. Venezia, D. Duca, M.A. Floriano, G. Deganello and A. Rossi, Surf. Interface Anal. 19 (1992) 543.
[14] A.M. Venezia, A. Rossi, D. Duca, A. Martorana and G. Deganello, Appl. Catal. 125 (1995) 113.
[15] G. Fagherazzi, A. Benedetti, A. Martorana, D. Duca, S. Giuliano and G. Deganello, Catal. Lett. 6 (1990) 263.
[16] A. Martorana, G. Deganello, D. Duca, G. Fagherazzi and A. Benedetti, J. Appl. Cryst. 25 (1992) 31.
[17] G. Fagherazzi, A. Benedetti, G. Deganello, D. Duca, A. Martorana and G. Spoto, J. Catal. 150 (1994) 117.
[18] M. Sernetz, H.R. Bittner, H. Williams and C. Baumhoer, in: The Fractal Approach to the Heterogeneous Catalysis, D. Avnir (Ed.) (John Wiley and Sons, Chichester, 1989) p. 361.
[19] A.A. Gorbunov, L.Y. Solovyova and V.A. Pasechik, J. Chomatogr. 448 (1988) 307.
[20] I. Halász and K. Martin, Angew. Chem. Int. Ed. Engl. 17 (1978) 901.
[21] E.F. Casassa, J. Polym. Sci. Part B 5 (1964) 773.
[22] E.F. Casassa and Y. Tagamy, Macromolecules 2 (1969) 14.
[23] E.F. Casassa, Macromolecules 9 (1976) 182.
[24] J. Janca, Adv. Chromatogr. 19 (1981) 37.

[25] R.N. Nikolov, J. Chromatogr. 364 (1984) 311.
[26] M.E. van Kreveld and N. van den Hoed, J. Chromatogr. 83 (1973) 111.
[27] A.G. Ogstone, Trans. Farady Soc. 54 (1958) 1754.
[28] B. Gelleri and M. Sernetz, Anal. Chim. Acta 163 (1984) 17.
[29] B.B. Mandelbrot, The Fractal Geometry of Nature, Freeman (Ed.) (S. Francisco, 1982).
[30] P. Pfeifer, in: Preparative Chemistry using Supported reagents, P. Laszlo (Ed.) (Academic Press, N.Y., 1987) p. 13.
[31] I. Halász and P. Vogtel, Angew. Chem. Int. Ed. Engl. 19 (1980) 24.
[32] W.H. Press, S.A. Teukolsky, W.T. Vetterling and B.P. Flammery, in: Numerical Recipes (Camb. U. Press, Cambridge, 1992).
[33] J. Schröder, GIT Fachz. Lab. 2 (1986) 1095.
[34] W.D. Ashton, in: Griffin's Statistical Monographs and Courses No. 32, A. Stuart (Ed.) (Griffin, London, 1972) p. 14.